Extended Kalman Filter-Based Active Alignment Control for LED Optical Communication

Pratap Bhanu Solanki, *Student Member, IEEE*, Mohammed Al-Rubaiai, and Xiaobo Tan, *Fellow, IEEE*

***Abstract*—Light-emitting diode (LED)-based optical communication is emerging as a low-power, low-cost, and high-data rate alternative to acoustic communication for mobile applications underwater. However, it requires a close-to-line-of-sight (LOS) link between the transmitter and the receiver. Alignment for maintaining LOS is challenging due to the constant movement of underlying mobile platforms caused by propulsion and unwanted disturbances. In this paper, we present a novel, compact LED-based communication system with active alignment control, in a two-dimensional setting, that maintains the LOS despite the underlying platform movement. An extended Kalman filter-based algorithm is proposed to estimate the angle between the receiver orientation and the receiver–transmitter line, which is used subsequently to adjust the receiver orientation. The algorithm uses only the measured light intensity from a single photodiode, where successive measurements are obtained via a scanning technique. A simple proportional controller is designed for alignment that also ensures the observability of the system. The effectiveness of the proposed active alignment algorithm is verified in simulation and experiments. In particular, its robustness in the presence of measurement noise is demonstrated via comparison with two alternative algorithms that are based on hill-climbing and three-point-averaging.**

***Index Terms*—Active alignment control, estimation and control, extended Kalman filter (EKF), light-emitting diode (LED) communication.**

I. Introduction

AUTONOMOUS underwater robots are used increasingly in marine sciences, environmental monitoring, and oil/gas exploration among other applications. Due to the heavy attenuation of radio frequency signals in water [1], acoustic communication has been the dominant method for underwater robots to communicate with each other and/or base stations. However, acoustic communication suffers from low data rates, high latency, and high power consumption [2]. Over the past few years, light-emitting diode (LED)-based optical communication has been proposed as a promising low-power, low-cost, high-rate solution for low-to-medium range underwater data transfer [3]–[5]. Several studies focused on increasing the range and data rates of LED communication. Brundage reported an optical communication system using a Titan blue lighting LED [6], which performed error-free communication over 1 Mb/s at distances up to 13 m. Doniec and Rus demonstrated a bidirectional underwater wireless communication system called AquaOptical II [7], which used 18 Luxeon Rebel LEDs and an avalanche photodiode and operated over a distance of 50 m at a data rate of 4 Mb/s.

An inherent challenge associated with the wireless optical communication is to establish and maintain close-to-line-of-sight links, as the light signals are highly directional. For many potential applications involving mobile platforms (in particular, underwater robots), maintaining a line-of-sight (LOS) is difficult due to movement of the platform caused by propulsion or ambient disturbances. Several approaches have been proposed to address the LOS requirement in optical communication systems. Pontbriand *et al.* used large-area photomultiplier tubes, to increase the field of view of the receiver [8]. Multiple LEDs and/or multiple photodiodes have been used to avoid the need of active pointing during optical-communication [7], [9]–[12]. These systems achieved the LOS through redundancy in transmitters and/or receivers, which resulted in a larger footprint, higher cost, and higher complexity.

In this paper, we present a compact LED communication system for a two-dimensional (2-D) setting, where a transceiver consists of a single LED and a single photodiode, and a rotating base for the transceiver enables the establishment and maintenance of the LOS between the communicating parties independent of the motions of the underlying robotic platforms. Furthermore, we propose an extended Kalman filter (EKF) for estimating the angle between the receiver orientation and the line connecting the receiver and the transmitter, which is then used to adjust the receiver orientation toward LOS. We note that Kalman filter and EKF have been proposed in optical beam steering in the context of laser-based free space optical communication, where the laser beam is considered as a single line and, thus, simple geometric relationships can be used to relate the measurement to the receiver/transmitter configuration [13], [14]. For example, in their simulation study, Soysal and Efe considered a quadrant photodetector as the measurement device, which was assumed to produce the signals directly proportional to azimuth and elevation errors [13]. Yoshida and Tsujimura

Manuscript received February 11, 2017; revised August 18, 2017; accepted May 17, 2018. Date of publication May 28, 2018; date of current version August 14, 2018. Recommended by Technical Editor S. Nahavandi. This work was supported by the National Science Foundation under Grant IIS 1319602, Grant ECCS 1446793, and Grant IIS 1734272. *(Corresponding author: Pratap Bhanu Solanki.)*

The authors are with the Department of Electrical and Computer Engineering, Michigan State University, East Lansing, MI 48824 USA (e-mail: prabhanu@msu.edu; alrubaia@msu.edu; xbtan@egr.msu.edu).

This paper has supplementary downloadable material available at http://ieeexplore.ieee.org provided by the authors.

Color versions of one or more of the figures in this paper are available online at http://ieeexplore.ieee.org.

Digital Object Identifier 10.1109/TMECH.2018.2841643

used a 2-D position-sensitive device and the detected beam spot position was geometrically related to the relative position and orientation between the transmitter and the receiver [14]. These approaches do not apply to our setting because of the diffusive nature of LED and the use of single photodetector in the proposed work.

We now briefly summarize our EKF-based alignment control approach. Based on a light intensity model, we first formulate an estimation problem, where the receiver estimates both its relative orientation to the transmitter and a quantity related to the overall light intensity at the receiver site. The rotating base is then instructed to move toward the alignment based on the estimated relative orientation. Due to the nonlinear nature of the observation function, an EKF is adopted for the state estimation. In order to ensure convergence of the EKF, light intensity measurements taken at two consecutive steps in the scanning motion are used in each state update. The feedback control algorithm then updates the orientation bias in the angular scan motion based on the state estimate.

Preliminary versions of parts of this paper were presented at the 2016 American Control Conference [15] and the 2016 IEEE International Conference on Advanced Intelligent Mechatronics [16], [17]. In addition to providing a comprehensive treatment of the system design, algorithm development, and simulation and experimental evaluation, this paper improves over the conference papers [15]–[17] in a number of ways. First, an analysis is presented for the design of the proportional control gain that ensures the nonsingularity of the observability matrix. Second, while the results in the previous conference versions were limited to a preliminary setup with a static receiver, in this paper, the performance of the proposed algorithm is evaluated with extensive simulation and experiments in a setting involving a mobile transmitter and a stationary receiver. Third, in these evaluations, we also compare the tracking performance of the EKF approach with two alternative schemes: hill-climbing and three-point averaging. Hill-climbing is a widely used, computationally efficient algorithm for optimization that locally updates the solution in the direction of higher objective function [18]. Since better alignment between the receiver and the LED leads to higher measured light intensity, the hill-climbing algorithm simply directs the receiver to keep moving in the direction of higher light intensity. The three-point-averaging algorithm, on the other hand, was first proposed in our earlier work [16], and it computes the next orientation of the receiver based on the weighted-average of three orientations: no change, a fixed rotation to the right, and a fixed rotation to the left, where the measured intensities at these orientations are used as weights. A performance metric is designed to evaluate and compare the three algorithms in terms of tracking effectiveness, where a range of measurement noise levels is considered. For each of the noise levels, multiple runs of simulation and the corresponding experiments have been performed to assess the average performance and simultaneously alleviate the effects of stochasticity on the results. It is found that the EKF algorithm significantly outperforms the alternatives in the presence of measurement noise.

The rest of this paper is organized as follows. In Section II, the design and hardware implementation of the LED communication system is described. In Section III, the model for the received light intensity is presented, followed by a state-space reformulation for the purpose of algorithm development. In Section IV, the estimation and tracking control algorithms are described. Simulation setup and results are presented in Section V, while experimental setup and results are discussed in Section VI. Finally, concluding remarks are provided in Section VII.

II. System Design and Implementation

An LED-based optical communication system mainly consists of two parts, the transmitter and the receiver. The transmitter converts the electrical signal into an optical signal. That signal passes through the medium and is picked up by the receiver. The receiver detects the optical signal and converts it back into an electrical signal for data processing. In addition to the transmitter and the receiver, the proposed system includes a mechanism for rotating the transmitter/receiver, to maintain the communication despite the movement of the underlying robotic platform. Considering the intended applications, small footprint and low power consumption are among the major design constraints.

A. System Components

The role of the optical transmitter is to convert the electrical signal into light pulses. Since the signal attenuation underwater is minimum in the wavelength range of 400–500 nm [19], an off-the-shelf blue LED (Cree XR-E Series LED from Cree Inc) is chosen, which provides 30.6 lm at 1 A and requires 3.3 V. It comes assembled with a heat sink. A circuit is designed to modulate the LED (turning it ON and OFF) in correlation with binary data. A photodiode from Advanced Photonix (part number PDB-V107) is chosen for the receiver, and it has high quantum efficiency at 410 nm, low dark current, and fast rise time (20 ns). A 12-V reverse bias across the photodiode is used to increase the bandwidth and quantum efficiency [20]. A transimpedance amplifier is used to convert the photodiode current signal into a voltage signal, which then goes through a filter for noise reduction.

The components of the transmitter and the receiver are placed on two printed-circuit boards (PCBs). The first PCB board is 2 inches in diameter and has two holes in the middle to attach set screw hubs for connecting to a motor shaft. The second PCB board has a rectangular shape with size of 1 inch $\times$ 2 inch, which holds the LED and the photodiode, and it is mounted perpendicularly to the first circular board by using four 90° header pins (see Fig. 1).

There are eight pins in the PCB circuits involving the power supply, the transmitted signal, and the received signal. These pins are connected by wires, which would be twisted when the PCBs are rotated. To address this problem, a slip ring (MT007 from MOFLON), an electromechanical device that allows the transmission of power and electrical signals from a stationary to a rotating structure, is adopted. A motor is used to rotate the device. We initially used a mini-dc motor equipped with a shaft

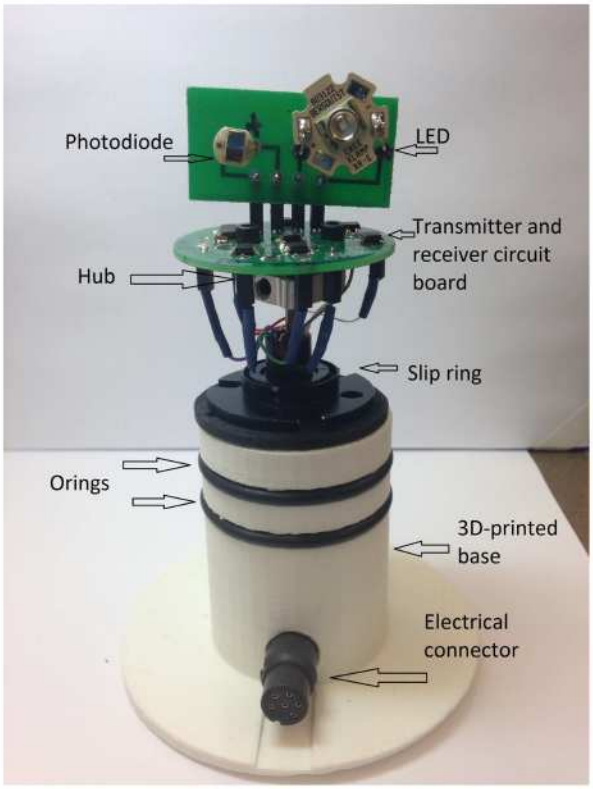

Fig. 1. Prototype of LED optical communication module with a rotational base.

encoder, but later switched to a stepper motor due to the higher control precision of the latter.

B. Characterization of Optical Communication Link Performance Underwater

We have conducted experiments in a swimming pool to examine the performance of the optical communication link when the transmitter and the receiver are aligned. The pool length is 23 m. The transmitter and the receiver are encapsulated in 10-cm-diameter PVC tubes (with a transparent window at the front) during the underwater experiments. Each of these tubes is then attached to another PVC tube that fixes the transmitter and receiver depth to 25 cm.

The light emitted from an LED spreads over a hemisphere shape. Conditioning optics are required to redistribute the LED light for specific requirements. Lenses are used for that purpose and currently, the most commonly used LED lens is the total internal retractor lens [21]. In our experiments, we use a 5° lens for the transmitter and the receiver. For each distance, experiments are performed five times to mitigate the impact of experimental errors. Fig. 2 shows that the signal strength declines when the distance between the receiver and the transmitter increases; however, there is an adequate signal strength (greater than 1 V) throughout the full length of the pool.

In addition to the signal strength measurements, we have also examined the data transmission performance of the system underwater. In the experiments, we use two computers to emulate two underwater robots and we connect them to the transmitter and the receiver, respectively, from the USB port using an

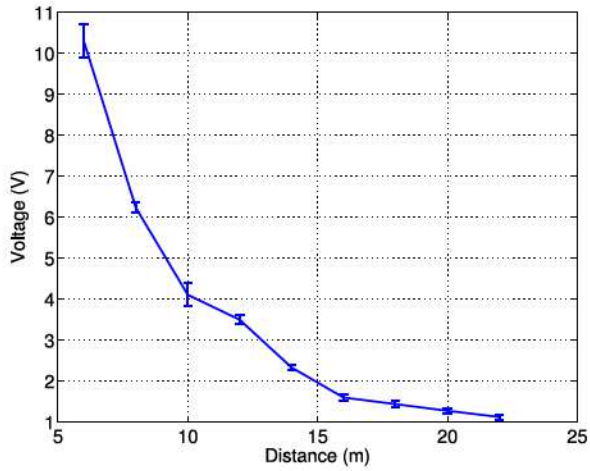

Fig. 2. Measured signal strength versus the transmitter–receiver distance in swimming pool experiments for the case of 5° lens for the transmitter. Vertical bars denote the standard deviations at each point of measurement.

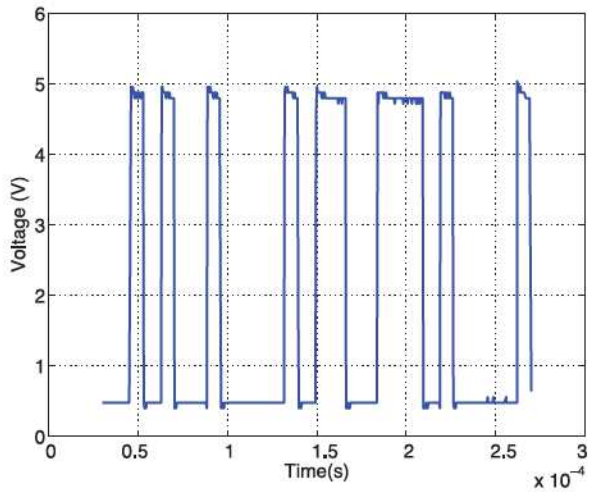

Fig. 3. Sample signal waveform captured during the communication bit error tests at a baud rate = 115 200 b/s.

FT232R USB-TTL level serial converter cable. The cable uses an FT232RQ chip, housed in the USB connector, to convert the USB data into asynchronous serial data at TTL levels. We send over 270 000 bytes five times at a distance of 22 m and receive those bytes on another computer. We confirm that the system is able to transmit and receive at a speed of 115.2 Kb/s with a bit error rate of zero. Fig. 3 shows an example of the received signal waveform.

The experimental results here are for the case when the transmitter and the receiver are stationary and aligned with each other. Clearly, this is not the case in the dynamic situation. In the rest of the paper, we focus on the problem of active alignment control between the receiver and the transmitter when there is a relative motion between them.

III. Modeling

In this section, we first review a light intensity model and then formulate the state-space model for an estimation problem, where, without the loss of generality, a scenario of two robots

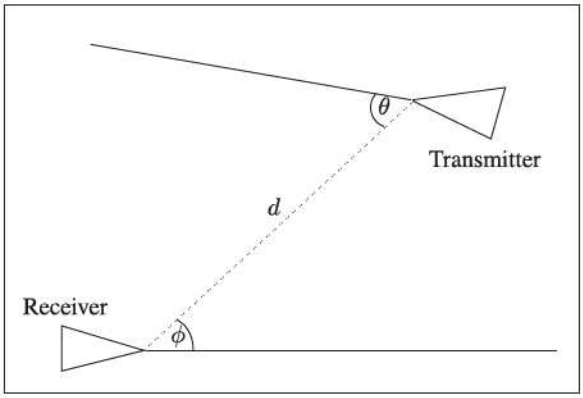

Fig. 4. Illustration of the relative position and orientation between the transmitter and the receiver.

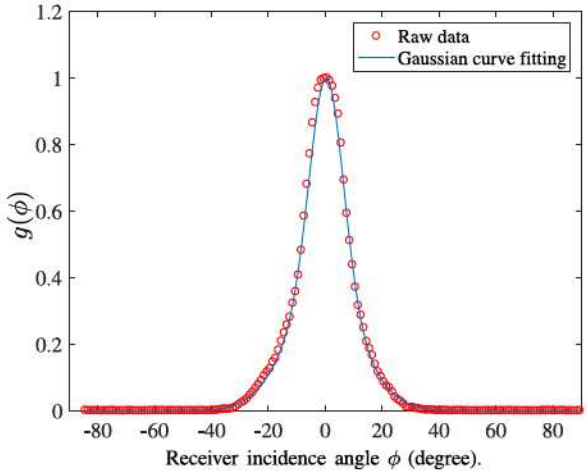

Fig. 5. Gaussian curve fitting for the function g for the photodiode used in this paper.

is considered. In addition, in this paper, we consider that the communicating parties are on the same plane.

A. Light Intensity Model

The model adopted here largely follows [22] with minor adjustments to suit the experimental prototype used in this paper. The model takes into account all stages of the transmitter and receiver circuits, including LED, lens, photodiode, and amplifiers. The model mainly describes the effect of relative position and orientation between the transmitter and the receiver on the signal strength. See Fig. 4 for an illustration of the variables of interest, including transmission angle θ, transmission distance d, and the angle of incidence ϕ.

The transmitter LED has an angular intensity distribution which is rotationally symmetric about the LED's normal ($\theta = 0°$). Thus, if we know the intensity of the LED along the normal, we can compute the intensity at other points at the same radial distance based on spatial intensity curve I_θ, which represents the light intensity at a unit distance for different transmitter angles. I_θ is maximum at $\theta = 0°$ and it rolls off as θ increases. Typically, I_θ can be obtained either directly from the LED vendor or measured experimentally.

To describe the extinction of the light signal we will adopt Beer's Law [23], which is used in understanding the attenuation in physical optics. Let c be the attenuation coefficient for the medium in which the light transmits. We assume that the coefficient is uniform across the entire length of transmission. Beer's law gives the exponential signal degradation at distance d caused by absorption

$$A = e^{-cd}. \tag{1}$$

By combining the effect of spherical spreading with exponential decay, we get the equation of the irradiance reaching the receiver site

$$E_\theta(d) = I_\theta e^{-cd}/d^2. \tag{2}$$

Finally, we need to consider the effect of angle of incidence ϕ, which is basically the angle made by the receiver normal with the line connecting the receiver to the transmitter. From [24], the power incident on the detector can be computed based on the signal irradiance at the detector position

$$P_{\text{in}} = E_\theta(d) A_0 g(\phi) \tag{3}$$

where A_0 denotes the detector area and $g(\phi)$ characterizes the dependence of the received light intensity on the incidence angle ϕ. The term $g(\phi)$ is setup dependent. For the receiver used in this paper, we have found the function $g(\phi)$ using Gaussian curve fitting of the normalized measurement data (see Fig. 5) collected at different orientations of the receiver. The resulting $g(\phi)$ takes the form of a bimodal Gaussian function

$$g(\phi) = a_1 e^{-\left(\frac{\phi - b_1}{c_1}\right)^2} + a_2 e^{-\left(\frac{\phi - b_2}{c_2}\right)^2} \tag{4}$$

where $a_1 = 0.6682$, $b_1 = 7.752$, $c_1 = 148.8$, $a_2 = 0.3340$, $b_2 = -13.57$, $c_2 = 325.8$ are the curve fitting parameters. The parameters b_1 and b_2 are relatively close to each other (over the range of $[-180°, 180°]$), so the resulting sum of the two modes has a single peak, as shown in Fig. 5. The curve fitting could be done using a single Gaussian mode but having one extra Gaussian mode gives significantly better fitting.

As the light arrives on the receiver photodiode, the photodiode produces a current, which gets filtered and amplified, to be processed by an analog–digital converter. After all the stages, the full signal strength model can be summarized as

$$V_d = C_p I_\theta e^{-cd} g(\phi)/d^2 \tag{5}$$

where V_d is the voltage signal and C_p is a constant of proportionality, which depends on the area of receiver photodiode and various parameters associated with the filter and amplifier circuits.

B. State-Space Problem Formulation

From Fig. 4 and (5), we can see that there are three independent variables θ, d, and ϕ that characterize the received light intensity. One could take these three variables as the states to be estimated by the system, and then try to drive them toward their desired values through control, if that is possible. However, often times the underlying robotic platforms are engaged in other

tasks and may not constrain or modify their motions to accommodate communication. For example, it may not be possible to change the distance d in a desirable way for communication since that would involve the movement of the robots. What is much more practical is to control the receiver angle ϕ, since it is a completely local decision due to the independent rotation base for the transceiver. In a two-way communication setting, since the transmitter and the receiver on each robot are pointing in the same direction, adjusting ϕ to zero on each robot automatically aligns each transmitter with the line connecting two robots. In light of this discussion, we can combine terms involving θ and d in a single variable and define the state variables as

$$\mathbf{x} \triangleq \begin{bmatrix} x_1 \\ x_2 \end{bmatrix} \triangleq \begin{bmatrix} C_p I_\theta e^{-cd}/d^2 \\ \phi \end{bmatrix}. \tag{6}$$

The value of x_1 is dependent on the distance and the transmission angle. In a typical scenario, the receiver does not have information about how the transmitter and its underlying robotic platform move. So in our case, we will assume that the relative dynamics between the two communicating robots is slow enough (quasi-static) that it can be captured with a Gaussian process. In particular, the dynamics of the states defined in (6) can be represented in the discrete-time domain as

$$\mathbf{x}_k \triangleq \begin{bmatrix} x_{1,k} \\ x_{2,k} \end{bmatrix} = \begin{bmatrix} x_{1,k-1} + w_{1,k-1} \\ x_{2,k-1} + u_k + w_{2,k-1} \end{bmatrix} \tag{7}$$

where k is the time index and $w_{1,k}$ and $w_{2,k}$ are the process noises assumed to be independent, white, Gaussian noises. These noise terms, to some extent, account for the slow dynamics of x_1 and x_2, which are not modeled explicitly. The term u_k is the control input through which the receiver angle is changed.

The kth measurement $V_{d,k}$ can be expressed in terms of the state variables, where an additive white Gaussian noise v_k, assumed to be independent from the process noises, is included

$$V_{d,k} = x_{1,k} g(x_{2,k}) + v_k. \tag{8}$$

Given the measurement, the goal is to estimate $x_{1,k}$ and $x_{2,k}$, based on which the control u_k is designed to drive x_2 toward $0°$, which is the orientation with the maximum light intensity.

IV. Estimation and Alignment Algorithms

Given that the measurement model (8) is nonlinear, a discrete time EKF [25] is explored for solving the estimation problem. From the (linear) state equation (7), the A and B matrices are

$$\begin{cases} A = \begin{bmatrix} 1 & 0 \\ 0 & 1 \end{bmatrix} \\ B = \begin{bmatrix} 0 \\ 1 \end{bmatrix}. \end{cases} \tag{9}$$

So that the system dynamics can be written as

$$\mathbf{x}_k = A\mathbf{x}_{k-1} + Bu_{k-1} + \mathbf{w}_{k-1} \tag{10}$$

with $\mathbf{w}_k = [w_{1,k}, w_{2,k}]^T$. Given that the output function in (8) is nonlinear, denoting the system's linearized output matrix at kth time instant as $C_k \triangleq C(\mathbf{x}_k)$, one can express the observability matrix at that time instant as [25]

$$\mathcal{O}_k = \begin{bmatrix} C_k \\ C_{k+1}A \end{bmatrix} = \begin{bmatrix} C_k \\ C_{k+1} \end{bmatrix}. \tag{11}$$

If the observability matrix $\mathcal{O}_k$ has a full rank of 2, the state estimation error under the EKF will be exponentially bounded in mean square and bounded with probability one under proper conditions [25]. A sufficient condition for $\mathcal{O}_k$ to be full rank is to make C_k a rank 2 matrix, which is only possible with at least two independent measurements of the light intensity. One could use two receivers with different orientations to address this problem, but that would increase the complexity and cost of the system. Instead, we introduce a scanning technique, where the motor of the rotating base is commanded to oscillate around a mean position. This mean position, which is what the control input modulates, is considered to be the state variable x_2 from here on.

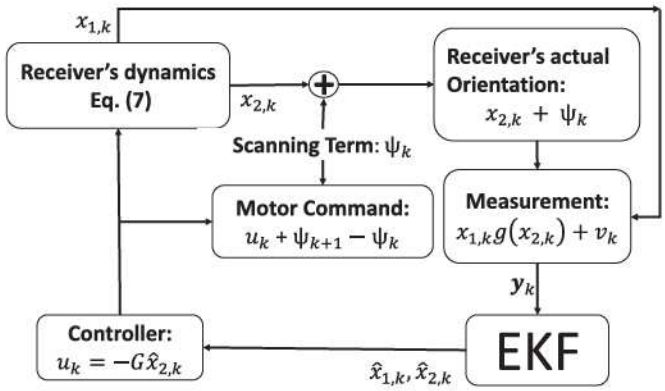

Fig. 6. Block diagram illustrating the proposed method.

Fig. 6 provides an outline of the proposed method. At each iteration, the states x_1 and x_2 are updated according to the system dynamics. The scanning term is added to account for the actual orientation of the receiver. The light intensity measured by the receiver is used by the EKF to update the state estimates. Next, the estimate $\hat{x}_2$ is used to compute the control term. We note that the focus of this paper is on the use of nonlinear estimation and basic feedback concepts to enable active alignment between the receiver and the LED. Therefore, exploration of advanced controllers is beyond the scope of this paper; for simplicity of implementation and presentation, a proportional controller is adopted. The final command sent to the motor is the sum of control term and the difference between the last two consecutive scanning terms.

Fig. 7 illustrates the scanning technique. The receiver oscillates through a defined array of angles $\Psi = \{\psi_1, \psi_2, \psi_3 \ldots \psi_n\}$, which contains predefined angles used for scanning. In our case $\Psi = \{-2°, -4°, -6°, -8°, -10°, -8°, -6°, -4°, -2°, 0°, 2°, 4°, 6°, 8°, 10°, 8°, 6°, 4°, 2°, 0°\}$. In each iteration, one ψ_k is chosen from this array sequentially. The measurement is taken at each ψ_k, and the last two measurements at ψ_k and ψ_{k-1} form

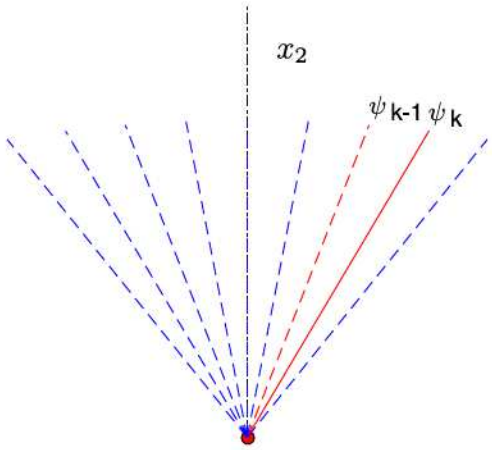

Fig. 7. Illustration of the receiver scanning sequence, with mean x_2 and last two angles of scanning ψ_k and ψ_{k-1}.

our output vector y

$$\mathrm{y}_k = \begin{bmatrix} x_{1,k} g(x_{2,k} + \psi_k) + v_k \\ x_{1,k-1} g(x_{2,k-1} + \psi_{k-1}) + v_{k-1} \end{bmatrix}. \tag{12}$$

Using the dynamics equation (7) and the measurement equation (12), an EKF can be implemented. The complete algorithm is explained as follows.

There are three covariance matrices, namely, P, Q and R, associated with an EKF. P is the conditional error covariance matrix and P^f represents the forecast of the covariance matrix. P^f needs to be initialized as a positive definite matrix. The initial value of the estimate of x_2 can be taken as $0°$. The initial value of the estimate of x_1 depends on the maximum possible value of intensity. A good choice of the initial estimate $\hat{x}_1$ would be from one-third to two-third of the maximum intensity value. Q is the process noise covariance matrix and R is the measurement noise covariance matrix. At step k,

1) *Prediction phase:* Both state estimates ($\hat{x}$) and error covariance matrix (P^f) are predicted

$$\hat{\mathrm{x}}_k^f \triangleq \begin{bmatrix} \hat{x}_{1,k}^f \\ \hat{x}_{2,k}^f \end{bmatrix} = \begin{bmatrix} \hat{x}_{1,k-1} \\ \hat{x}_{2,k-1} + u_{k-1} \end{bmatrix} \tag{13}$$

$$P_k^f = AP_{k-1}A^T + Q \tag{14}$$

where $\hat{x}_{m,k}^f$ denotes the estimate of the mth state at kth interval and the superscript f stands for "forecast."

2) *Estimated output:* From (12), the estimated output can be written as

$$\hat{\mathrm{y}}_k \triangleq \begin{bmatrix} \hat{y}_{1,k} \\ \hat{y}_{2,k} \end{bmatrix} \triangleq \begin{bmatrix} \hat{x}_{1,k}^f g(\hat{x}_{2,k}^f + \psi_k) \\ \hat{x}_{1,k-1} g(\hat{x}_{2,k-1} + \psi_{k-1}) \end{bmatrix}. \tag{15}$$

With (13), one can write

$$\hat{\mathrm{y}}_k = h(\hat{x}_{1,k}^f, \hat{x}_{2,k}^f) \triangleq \begin{bmatrix} \hat{x}_{1,k}^f g(\hat{x}_{2,k}^f + \psi_k) \\ \hat{x}_{1,k}^f g(\hat{x}_{2,k}^f - u_{k-1} + \psi_{k-1}) \end{bmatrix}. \tag{16}$$

The term u_{k-1} would be expressed in terms of the state variables later. Now, the linearized observation matrix C_k can be computed as

$$C_k = \frac{\partial h(\hat{x}_{1,k}^f, \hat{x}_{2,k}^f)}{\partial \hat{\mathrm{x}}_k^f} = \begin{bmatrix} C_{k,1,1} & C_{k,1,2} \\ C_{k,2,1} & C_{k,2,2} \end{bmatrix} \tag{17}$$

where

$$C_{k,1,1} = g(\hat{x}_{2,k}^f + \psi_k)$$
$$C_{k,1,2} = \hat{x}_{1,k}^f g'(\hat{x}_{2,k}^f + \psi_k)$$
$$C_{k,2,1} = g(\hat{x}_{2,k}^f - u_{k-1} + \psi_{k-1})$$
$$C_{k,2,2} = \hat{x}_{1,k}^f g'(\hat{x}_{2,k}^f - u_{k-1} + \psi_{k-1})$$

with $g'(\cdot)$ being the derivative of $g(\cdot)$ with respect to its argument.

3) Update/analysis phase:

$$K_k = P_k^f C_k^T (C_k P_k^f C_k^T + R)^{-1} \tag{18}$$

$$\hat{\mathrm{x}}_k = \hat{\mathrm{x}}_k^f + K_k(\mathrm{y}_k - \hat{\mathrm{y}}_k) \tag{19}$$

$$P_k = (I - K_k C_k) P_k^f. \tag{20}$$

It is to be noted that P_k and $\hat{\mathrm{x}}_k$ without any superscripts denote the updated values after the analysis phase.

4) Finally, the control is computed as

$$u_k = -G\hat{x}_{2,k} \tag{21}$$

where G is a positive gain, which, motivated by the goal of driving the mean of scan x_2 to zero. The final rotation angle sent to the motor is $u_k + \psi_{k+1} - \psi_k$, which will be used to update the receiver angle at time $k+1$.

Since the algorithm is based on EKF, the convergence depends mainly on two factors: the full rank condition of the observability matrix $\mathcal{O}_k$ of the linearized system [recall (11)], and the initial conditions of the state estimates, which were already discussed earlier. Since the full rank condition of $\mathcal{O}_k$ is ensured by the nonsingularity of the output matrix C_k, we consider the determinant of C_k

$$|C_k| = \hat{x}_{1,k}^f g(\hat{x}_{2,k}^f + \psi_k) g'(\hat{x}_{2,k}^f - u_{k-1} + \psi_{k-1}) - \hat{x}_{1,k}^f g(\hat{x}_{2,k}^f - u_{k-1} + \psi_{k-1}) g'(\hat{x}_{2,k}^f + \psi_k).$$

Using (13) and (21), we obtain

$$u_{k-1} = -\frac{G\hat{x}_{2,k}^f}{1-G}$$

which implies

$$\hat{x}_{2,k}^f - u_{k-1} = \frac{\hat{x}_{2,k}^f}{1-G}$$

and thus

$$|C_k| = \hat{x}_{1,k}^f g(\hat{x}_{2,k}^f + \psi_k) g'\left(\frac{\hat{x}_{2,k}^f}{1-G} + \psi_{k-1}\right) - \hat{x}_{1,k}^f g\left(\frac{\hat{x}_{2,k}^f}{1-G} + \psi_{k-1}\right) g'(\hat{x}_{2,k}^f + \psi_k).$$

Since x_1 represents the light intensity at the receiver site (which is in general different from the measured intensity by the receiver), it is always positive—if x_1 were zero, there would not be any measured signal even if the receiver is perfectly pointing at the transmitter and the algorithm would be stopped. Therefore, it is reasonable to assume $\hat{x}^f_{1,k} > 0$. Thus, the only possibility for $|C_k| = 0$ is then

$$g(\hat{x}^f_{2,k} + \psi_k)g'\left(\frac{\hat{x}^f_{2,k}}{1-G} + \psi_{k-1}\right)$$
$$-g\left(\frac{\hat{x}^f_{2,k}}{1-G} + \psi_{k-1}\right)g'(\hat{x}^f_{2,k} + \psi_k) = 0$$

or

$$\frac{g'(\hat{x}^f_{2,k} + \psi_k)}{g(\hat{x}^f_{2,k} + \psi_k)} = \frac{g'(\frac{\hat{x}^f_{2,k}}{1-G} + \psi_{k-1})}{g(\frac{\hat{x}^f_{2,k}}{1-G} + \psi_{k-1})}. \tag{22}$$

One can show that the function $\mathbf{G} = \frac{g'(\cdot)}{g(\cdot)}$ is monotonously decreasing in our domain of interest: $(-180°, 180°)$. Hence, (22) would be true if and only if

$$\hat{x}^f_{2,k} + \psi_k = \frac{\hat{x}^f_{2,k}}{1-G} + \psi_{k-1} \tag{23}$$

which implies

$$\hat{x}^f_{2,k} = \frac{(1-G)}{G}(\psi_k - \psi_{k-1}). \tag{24}$$

Since

$$|\hat{x}^f_{2,k}| < 180 \text{ and } |\psi_k - \psi_{k-1}| = 2$$

a sufficient condition for guaranteeing that (24) does not hold and thus C_k is nonsingular is

$$\left|\frac{1-G}{G}\right| < 90, \text{ or } G > \frac{1}{91}.$$

Here, we get a very relaxed criterion on G. Thus, for our simulation and experiments, we used $G = 0.5$.

V. Simulation Results

In this section, we verify the effectiveness of our algorithm through MATLAB simulation. In addition, we introduce two alternative algorithms, followed by a comparison of EKF with the two algorithms.

To further explore the effect of unmodeled system dynamics (which were ignored in the algorithm development, considering that the receiver typically would not have access to the motion information of the transmitter), we have included some arbitrary dynamics for the system in the simulation. Specifically, the system state evolves according to the following:

$$\begin{cases} x_{1,k} = x_{1,k-1} + w_{1,k-1} \\ x_{2,k} = x_{2,k-1} + \beta + u_{k-1} + w_{2,k-1} \end{cases} \tag{25}$$

where β is an unknown constant disturbance. The term β corresponds to the relative angular movement between the transmitter and the receiver, and it simulates the scenario where the transmitter revolves around the receiver while shining directly at it.

TABLE I
Parameters Associated With EKF Implementation in the Simulation

Parameter	Description	Value
$\hat{\mathbf{x}}_0$	Initial state estimate	$[2, 0]^T$
P_0^f	Initial error covariance matrix	$\begin{bmatrix} 100 & 0 \\ 0 & 1000 \end{bmatrix}$
Q_{sys}	System's process noise covariance matrix	$\begin{bmatrix} 0.0025 & 0 \\ 0 & 0.01 \end{bmatrix}$
Q	EKF's process noise covariance matrix	$\begin{bmatrix} 0.25 & 0 \\ 0 & 1 \end{bmatrix}$
R_{sys}	System's measurement noise covariance matrix	$\begin{bmatrix} 0.04 & 0 \\ 0 & 0.04 \end{bmatrix}$
R	EKF's measurement noise covariance matrix	$\begin{bmatrix} 1 & 0 \\ 0 & 1 \end{bmatrix}$
G	Proportional controller gain	0.5

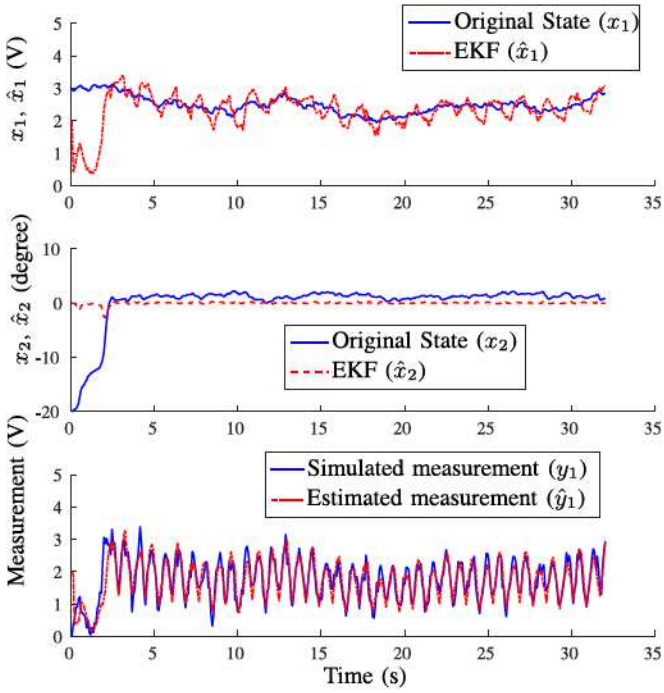

Fig. 8. Simulation results of EKF when the x_2 dynamics contains an unknown constant disturbance $\beta = 1.2°/\text{s}$.

Based on the model and the algorithms described earlier, the simulation is conducted with parameters listed in Table I. Note that we have used different Q and R values for EKF, than the system's noise covariance matrices, as it is shown earlier [15] that using scaled-up noise covariance matrices for EKF implementation gives an improvement in convergence performance.

Fig. 8 shows the results obtained from a simulation run with $\beta = 1.2$. From Fig. 8, it can be seen that the estimated states converge to the neighborhood of the original states in about 2 s and remain there throughout the run. We note that the estimated value for the state x_2 is slightly lower than the actual. Most likely this can be attributed to the positive bias term β in the system dynamics, which constantly produces a shift of receiver

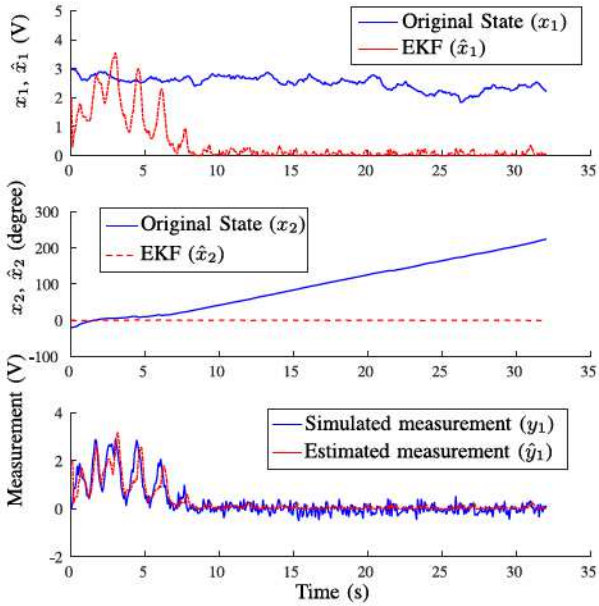

Fig. 9. Simulation results of EKF method's failure when the unknown constant rate disturbance β is increased to $8^\circ/\text{s}$.

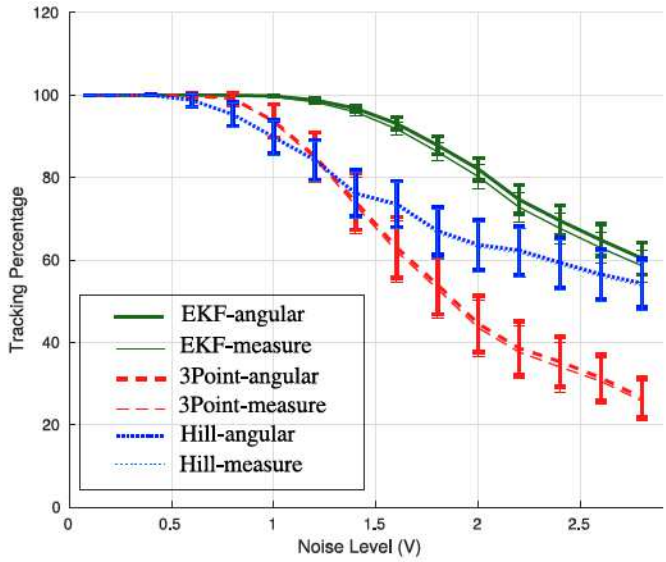

Fig. 10. Simulation results on comparison of alignment control performance for the three methods, for different levels of measurement noise, when system states are evolved according to (25) with $\beta = 1.2$. Vertical bars denote the down-scaled standard deviations at each point. "Hill" represents the hill-climbing algorithm, and "3Point" represents the three-point-averaging algorithm.

orientation in the positive direction. Note that the oscillations in the measurements are attributed to the scanning motion of the receiver. And we note that the actual mean (state x_2) converges to the neighborhood of zero in about 2–3 s. This corresponds to the alignment of the mean direction of the receiver to the direction that faces the transmitter.

To explore the limit of algorithm's assumption on quasi-static dynamics, the constant disturbance term β is increased to an extent where the tracking fails. Fig. 9 shows the states when the EKF algorithm stops working and the angle of incidence x_2 starts going unbounded. This corresponds to the receiver's direction moving away from the transmitter-facing direction.

Next, we compare the performance of the EKF-based algorithm with two alternative algorithms: hill-climbing and three-point averaging. In particular, we explore the performance of the algorithms in the presence of measurement noises. In hill-climbing, the receiver starts with an orientation, measures the light intensity, and rotates by angle $\gamma = 2^\circ$ in either the clockwise or counterclockwise direction. It then measures the new light intensity. If the latter is higher than the previous value, it will rotate by γ again in the same direction; otherwise it will rotate in the opposite direction.

For the three point-averaging algorithm [24], the receiver performs a clockwise rotation and then a counterclockwise rotation by an angle γ from the original location. Meanwhile, it takes the light intensity measurements at each step (V_1, V_2, V_3), where V_1, V_2, V_3 represent the voltages at the clockwise rotation, counterclockwise rotation, and original location ($\gamma = 0$), respectively. The new turning angle γ_p of the rotating base is calculated by taking a weighted average of these signals at three steps

$$\gamma_p = \frac{\gamma V_1 - \gamma V_2}{V_1 + V_2 + V_3}. \tag{26}$$

The algorithm is implemented in MATLAB for simulation, with turning angle $\gamma = 2^\circ$. To quantify the alignment control performance, two metrics are considered based on the angle of incidence ϕ and the clean light intensity measurement (light intensity value uncorrupted by noise v_k, defined as "clean measurement"), respectively. Note that the algorithms use the noise-corrupted measurement for alignment control, and the clean measurement is used only for performance evaluation. We define the "tracking percentage" as the fraction of time when the system is in the tracking zone, where the latter could be determined based on either the angle of incidence or the clean measurement. In particular, we consider a threshold of 15° for the angle of incidence ϕ : if ϕ is outside the range $[-15, 15]^\circ$, it would be considered out of the tracking zone. From Fig. 5, we can see that this angular threshold corresponds to about 20% of the maximum level of the intensity, which we will use as a threshold for the "clean measurement" for determining whether the receiver orientation is in the tracking zone. For a maximum intensity of 3 V, the corresponding intensity threshold for tracking is 0.6 V.

For the comparison of alignment control performance, each algorithm is run with a series of noise levels for the measurement. As the noise level increases, the stochasticity in the tracking percentage increases. Hence in simulation, for each noise level, results of 1000 runs have been combined. In each run, the tracking percentage is computed and then the average over the 1000 runs is obtained to get an estimate of the expected value. The standard deviation in each case is also computed to capture the variation among the runs. Fig. 10 shows the plots for the mean of each algorithm with standard deviation as error bars. For clarity, the standard deviation in error bars is scaled down by five times. For each of the algorithm, the tracking percentage is

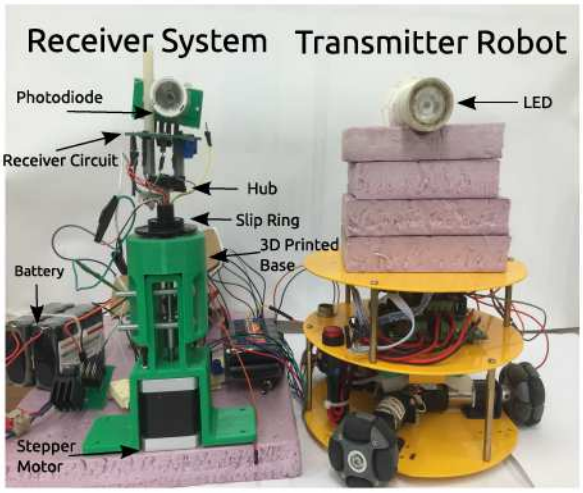

Fig. 11. Complete setup: Receiver(left) on a rotation base and transmitter LED on a mobile robot (right).

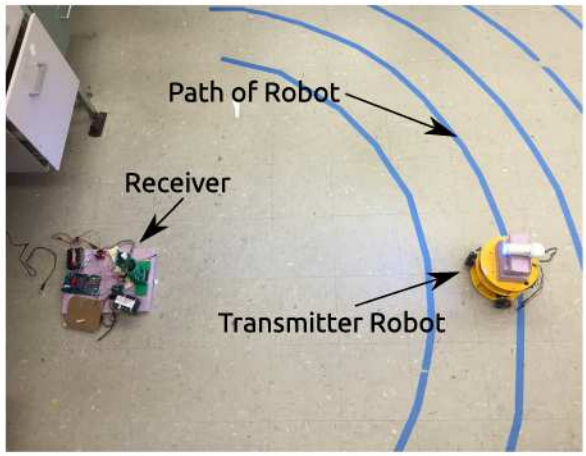

Fig. 12. Experimental setup: Transmitter robot moving around static receiver, following the marker lines.

computed by the two methods (based on the angle of incidence (ϕ), legend "-angular," and the light intensity measurement, legend "measure") mentioned earlier.

The purpose of using two methods to compute tracking is to show that there is a high amount of correlation between the tracking percentages computed by these two methods. So that in the case of experiments, even if the angular data are not available, we can confidently rely on the tracking percentage generated by the intensity measurement data. From Fig. 10, one can easily see that the tracking performance of the EKF-based algorithm is much better than that of the other two. The tracking remains 100% even at the noise level of 1.0 and it decreases gradually after that, which gives a good range of operation. The other two algorithms perform well under low noise levels, but their performance degrades faster than the EKF at higher noise levels. It can also be observed that the standard deviation under the EKF-based algorithm is also much lower than the other two algorithms, which further proves its reliability under higher noise levels.

VI. Experimental Results

In this section, we verify the efficacy of our algorithm by implementing cases similar to the simulation on an experimental setup. While the LED communication hardware design allows us to use both the receiver and the transmitter in the same module at once, so that two robots, each equipped with such a module, can communicate with each other both-ways, in this particular work we are focused on implementation of tracking algorithm on the receiver. Therefore, a separate light source is used as a transmitter. Fig. 11 shows such a transmitter–receiver pair used in the experiments. The transmitter is mounted on a mobile robot to facilitate the relative motion with respect to the receiver. It is to be noted that the receiver in Fig. 11 is a modified version of the device shown in Fig. 1. Here, as mentioned earlier, a stepper motor is used instead of a dc motor. The stepper motor has a precise control over the angular position. For the real-time onboard implementation of all computations, Intel Edison mini-computer board is used. It is equipped with 500-MHz Atom 2-Core CPU and 1 GB of LPDDR3 RAM. The hardware specifications are sufficient for the real-time computation required for our algorithm, and each EKF iteration takes about 50 ms to complete.

A mobile robot equipped with the transmitter revolves around the static receiver at a distance of 1.25 m while facing the receiver (see Fig. 12). Here, the transmitter robot is hard-coded to follow the circular path centered around the receiver, which not only ensures the distance d to be constant but also enables the transmitter to focus light on the receiver throughout the run ($\theta \approx 0^\circ$). The robot's speed is fixed in such a way so that it revolves around the receiver at $1^\circ/\text{s}$. On the receiver's end, an averaging filter is implemented on the on-board measurement of the light intensity. Currently, our experiments are conducted in the air so the noise is relatively small and can be removed by averaging. The averaged output of the filter is termed as "clean measurement" for the experiments. Moreover, to implement a range of noises, an extra artificial Gaussian noise term is added to the clean measurement.

Fig. 13 shows the evolution of state estimates and measurement output for a particular run with the additional, artificial noise level of 1.0 when the EKF-based algorithm is implemented. Here, we can see that the estimate of the mean of the scan ($\hat{x}_2$) goes to a bounded neighborhood of zero as well. It is to be noted that we do not have access to the original states of the system, hence only the estimates are plotted. However, while running the experiment, we have visually observed that after a few iterations, the mean angular position of the receiver-scan starts aligning itself with the line connecting the transmitter to the receiver, which implies that the real x_2 also converges to the neighborhood of 0°. Moreover, the estimate $\hat{x}_1$ stays within a relatively narrow range (according to our design of experiment), which should be close to the actual x_1. Hence, according to these observations, the estimates remain within a close range around the original states.

To conduct a comparison between the three algorithms, we further perform multiple runs in the experiment. However, unlike simulation, it is not practical to do 1000 runs in the

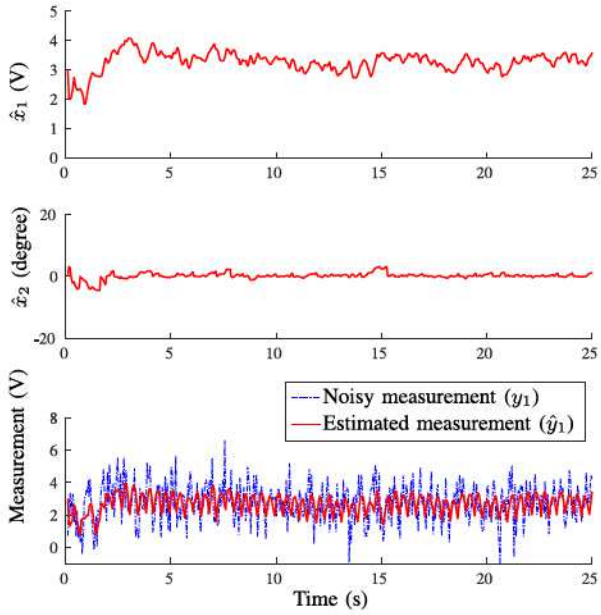

Fig. 13. Experimental results when the transmitter robot moves around the receiver with an angular rate of about 1 °/s. The measurements are corrupted with the noise level of 1.0.

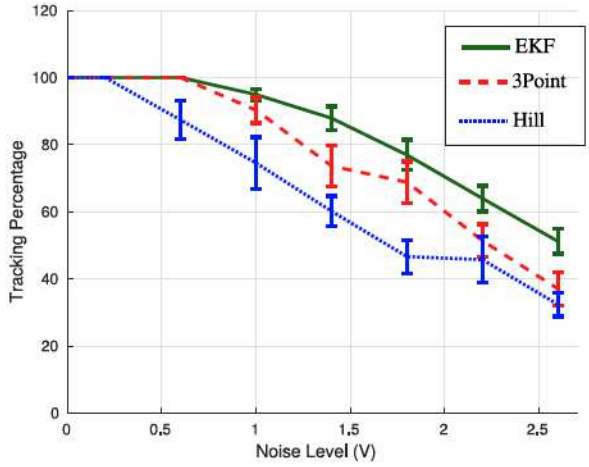

Fig. 14. Experimental results on comparison of alignment control performance for the three methods, for different levels of measurement noise when the constant disturbance (β) is $2.8°/s$. Vertical bars denote the downscaled standard deviations at each point.

experiments for each case, and we limit the number of experiments to 10 runs. Moreover, when the transmitter robot moves along the circular path, its trajectory is not always consistent. For instance, sometimes it goes a little closer to the receiver and sometimes further. The data generated by this motion is good for qualitative demonstration, but to have a fair quantitative comparison between the algorithms, we need a consistent system. Hence, we choose to keep the transmitter robot static and introduce an unknown constant disturbance term, similar to β in (25) in the onboard program. This disturbance term forces the receiver to rotate away from the transmitter facing direction. Fig. 14 shows the plot of the tracking percentage with scaled-down standard deviation error-bars over the range of noise level. It is to be noted that since the angular data is not available, the tracking is computed by thresholding of light intensity measurements. As we can see, the behaviors of the algorithms in the experiment are similar to those observed in simulation and the EKF algorithm has higher tracking performance with gradual degradation as compared to other two algorithms. The variance in the tracking percentage of EKF is also lower than the other two alternative algorithms. Other than the comparative performance evaluation, if we consider the noise level of 1.0, which is one-third of the maximum intensity or 22 dB signal to noise ratio, we have more than 95% of tracking.

VII. Conclusion and Future Work

In this paper, a compact LED-based communication system using a single receiver with active alignment control has been presented. For tracking, we have tested the applicability of simpler algorithms like the hill-climbing and the three-point averaging methods. These methods are good for low noise environments, but their performance degrades steeply at higher noise scenarios. Whereas a principled approach using state estimation and control like our proposed EKF-based alignment control algorithm not only gives comparable results in lower noise cases, but performs robustly in the case of higher noise environment. In our approach, the motion of the transmitter was assumed to be unknown and captured as part of a white Gaussian noise. A scanning technique is implemented to satisfy the observability criterion required for the EKF. A simple proportional controller is used for active alignment.

As mentioned in Section IV, the main focus of this paper was to demonstrate the instrumental role of nonlinear estimation and feedback control in the active alignment of the LED and the receiver. In particular, this approach uses the measurement history to estimate the state variables and subsequently applies a control action based on the state estimate. It outperforms algorithms that simply react to the current measurement (such as the hill-climbing and three-point-averaging algorithms) in the presence of measurement noises, at a modest cost of implementation complexity. While the EKF was adopted for state estimation, it was not meant to be the only or best possible choice. Other tools, such as the unscented Kalman filter [26] and the moving horizon estimator [27], could also work well for this problem. Similarly, while a simple proportional controller showed reasonably good performance, we anticipate that more advanced controllers, such as PID control or sliding mode control, could deliver even better performance at the cost of complexity.

For future work, we plan to explore the effectiveness of the proposed system in the underwater setting, which motivated the LED-based optical communication in the first place. In particular, we will mount the communication modules on two underwater robots, and investigate the improvement of the algorithm to address additional challenges introduced by water disturbances and robot motion. Moving forward, we will also extend the system to the 3-D setting, where the robots can move underwater in any direction and the transceivers of robots need to align themselves a in 3-D spatial setting, to establish and maintain the line of sight for communication.

REFERENCES

[1] L. Butler, "Underwater radio communication," *Amateur Radio*, 1987.

[2] S. Climent, A. Sanchez, J. V. Capella, N. Meratnia, and J. J. Serrano, "Underwater acoustic wireless sensor networks: Advances and future trends in physical, MAC and routing layers," *Sensors*, vol. 14, no. 1, pp. 795–833, 2014.

[3] F. Hanson and S. Radic, "High bandwidth underwater optical communication," *Appl. Opt.*, vol. 47, no. 2, pp. 277–283, Jan. 2008.

[4] R. Hagem, D. V. Thiel, S. O'Keefe, A. Wixted, and T. Fickenscher, "Low-cost short-range wireless optical FSK modem for swimmers feedback," in *Proc. IEEE Sensors Conf.*, Oct. 2011, pp. 258–261.

[5] F. Lu, S. Lee, J. Mounzer, and C. Schurgers, "Low-cost medium-range optical under water modem: Short paper," in *Proc. 4th ACM Int. Workshop UnderWater Netw.*, 2009, pp. 11:1–11:4.

[6] H. Brundage., "Designing a wireless underwater optical communication system," Master's thesis, Massachusetts Inst. Technol., Cambridge, MA, USA, 2010.

[7] M. Doniec and D. Rus, "Bidirectional optical communication with AquaOptical II," in *Proc. IEEE Int. Conf. Commun. Syst.*, Nov. 2010, pp. 390–394.

[8] C. Pontbriand, N. Farr, J. Ware, J. Preisig, and H. Popenoe, "Diffuse high-bandwidth optical communications," in *Proc. OCEANS*, Sep. 2008, pp. 1–4.

[9] D. Anguita, D. Brizzolara, and G. Parodi, "Building an underwater wireless sensor network based on optical communication: Research challenges and current results," in *Proc. 3rd Int. Conf. Sensor Technol. Appl.*, 2009, pp. 476–479.

[10] D. Anguita, D. Brizzolara, and G. Parodi, "Optical wireless communication for underwater wireless sensor networks: Hardware modules and circuits design and implementation," in *Proc. OCEANS*, 2010, pp. 1–8.

[11] I. Rust and H. Asada, "A dual-use visible light approach to integrated communication and localization of underwater robots with application to non-destructive nuclear reactor inspection," in *Proc. IEEE Int. Conf. Robot. Autom.*, May 2012, pp. 2445–2450.

[12] J. Simpson, B. Hughes, and J. Muth, "Smart transmitters and receivers for underwater free-space optical communication," *IEEE J. Sel. Areas Commun.*, vol. 30, no. 5, pp. 964–974, Jun. 2012.

[13] G. Soysal and M. Efe, "Kalman filter aided cooperative optical beam tracking," *Radioengineering*, vol. 12, no. 2, pp. 242–248, Jun. 2010.

[14] K. Yoshida and T. Tsujimura, "Tracking control of the mobile terminal in an active free-space optical communication system," in *Proc. SICE-ICASE Int. Joint Conf.*, Oct. 2006, pp. 369–374.

[15] P. B. Solanki, M. Al-Rubaiai, and X. Tan, "Extended Kalman filter-aided alignment control for maintaining line of sight in optical communication," in *Proc. Amer. Control Conf.*, Jul. 2016, pp. 4520–4525.

[16] M. Al-Rubaiai and X. Tan, "Design and development of an LED-based optical communication system with active alignment control," in *Proc. IEEE Int. Conf. Adv. Intell. Mechatronics*, Jul. 2016, pp. 160–165.

[17] P. B. Solanki and X. Tan, "Experimental implementation of extended Kalman filter-based optical beam tracking with a single receiver," in *Proc. IEEE Int. Conf. Adv. Intell. Mechatronics*, Jul. 2016, pp. 1103–1108.

[18] S. J. Russell and P. Norvig, *Artificial Intelligence: A Modern Approach*, 2nd ed. London, U.K.: Pearson Education, 2003.

[19] S. N. White, A. D. Chave, and G. T. Reynolds, "Investigations of ambient light emission at deep-sea hydrothermal vents," *J. Geophys. Res., Solid Earth*, vol. 107, no. B1, pp. EPM 1-1–EPM 1-13, 2002.

[20] S. B. Alexander, *Optical Communication Receiver Design*. Bellingham, WA, USA: SPIE, 1997.

[21] J. Jiang, S. To, W. Lee, and B. Cheung, "Optical design of a freeform TIR lens for LED streetlight," *Optik—Int. J. Light Electron Opt.*, vol. 121, no. 19, pp. 1761–1765, 2010.

[22] M. Doniec, M. Angermann, and D. Rus, "An end-to-end signal strength model for underwater optical communications," *IEEE J. Ocean. Eng.*, vol. 38, no. 4, pp. 743–757, Oct. 2013.

[23] F. Miller, A. Vandome, and J. McBrewster, *Beer-Lambert Law*. Saarbrücken, Germany: VDM Publishing, 2009.

[24] M. Al-Rubaiai, "Design and development of an LED-based optical communication system," Master's thesis, Michigan State Univ., East Lansing, MI, USA, Aug. 2015.

[25] K. Reif, S. Gunther, E. Yaz, and R. Unbehauen, "Stochastic stability of the discrete-time extended Kalman filter," *IEEE Trans. Autom. Control*, vol. 44, no. 4, pp. 714–728, Apr. 1999.

[26] S. J. Julier and J. K. Uhlmann, "A new extension of the Kalman filter to nonlinear systems," in *Proc. Int. Symp. Aerosp./Defense Sens., Simul. Controls*, Orlando, FL, USA, 1997, pp. 182–193.

[27] E. L. Haseltine and J. B. Rawlings, "Critical evaluation of extended Kalman filtering and moving-horizon estimation," *Ind. Eng. Chem. Res.*, vol. 44, no. 8, pp. 2451–2460, 2005.

Pratap Bhanu Solanki (S'17) received the B.Tech. degree in electrical engineering from the Indian Institute of Technology Kanpur, Kanpur, India, in 2013. He is currently working toward the Ph.D. degree in electrical and computer engineering at Michigan State University, East Lansing, MI, USA.

His research focusses on alignment control of LED-based optical communication systems for underwater applications.

Mohammed Al-Rubaiai received the B.S. degree in mechatronics engineering from the University of Baghdad, Baghdad, Iraq, in 2009, and the M.S. degree in electrical engineering from Michigan State University, East Lansing, MI, USA, in 2015. He has been working toward the Ph.D. degree at the Smart Microsystems Laboratory, Department of Electrical and Computer Engineering, Michigan State University, since August 2016.

His current research is focused on soft robotics.

Dr. Al-Rubaiai is a student member of ASME.

Xiaobo Tan (S'97–M'02–SM'11–F'17) received the B.Eng. and M.Eng. degrees in automatic control from Tsinghua University, Beijing, China, in 1995 and 1998, respectively, and the Ph.D. degree in electrical and computer engineering from the University of Maryland, College Park, MD, USA, in 2002.

From September 2002 to July 2004, he was a Research Associate with the Institute for Systems Research, University of Maryland. In 2004, he joined the Department of Electrical and Computer Engineering, Michigan State University (MSU), East Lansing, MI, USA, as a faculty, where he is currently an MSU Foundation Professor. He has coauthored one book *Biomimetic Robotic Artificial Muscles* (World Scientific Publishing Co Pte Ltd, Singapore) and more than 200 peer-reviewed journal and conference papers, and holds three U.S. patents. His research interests include modeling and control of systems with hysteresis, electroactive polymer sensors and actuators, soft robotics, and bio-inspired underwater robots and their application to environmental sensing.

Prof. Tan has served as an Associate Editor/Technical Editor for *Automatica*, IEEE/ASME TRANSACTIONS ON MECHATRONICS, and *International Journal of Advanced Robotic Systems*, and also served as the Program Chair of the 2011 International Conference on Advanced Robotics and the General Chair of the 2018 ASME Dynamic Systems and Control Conference. He was the recipient of NSF CAREER Award in 2006, the MSU Teacher-Scholar Award in 2010, the MSU College of Engineering Withrow Distinguished Scholar Award in 2018, the Distinguished Alumni Award from the Department of Electrical and Computer Engineering, University of Maryland in 2018, and several best paper awards.